Analytical Methods

Measuring Stimulation and Inhibition of Intracellular Nitric Oxide Production in SIM-A9 Microglia using Microfluidic Single Cell Analysis

Journal:	*Analytical Methods*
Manuscript ID	AY-ART-08-2020-001578
Article Type:	Paper
Date Submitted by the Author:	10-Jun-2018
Complete List of Authors:	Sibbitts, Jay; Kansas State University, Chemistry Culbertson, Christopher; Kansas State University, Department of Chemistry

ARTICLE

Measuring Stimulation and Inhibition of Intracellular Nitric Oxide Production in SIM-A9 Microglia using Microfluidic Single Cell Analysis

Received 00th January 20xx,
Accepted 00th January 20xx

DOI: 10.1039/x0xx00000x

Jay Sibbitts[a] and Christopher T. Culbertson[a]*

Chronic neuroinflammation has long been considered to be a central factor in accelerating the progression of neurodegenerative diseases such as Alzheimer's diseases, Parkinson's disease and chronic traumatic encephalopathy. Under pathological conditions microglia produce inflammatory signaling molecules, such as nitric oxide (NO), that can damage DNA and proteins and ultimately induce neuronal apoptosis. One strategy for treating neurodegenerative diseases is to specifically target NO production through inhibition of inducible nitric oxide synthase (iNOS). However, accurately measuring changes in microglial NO production in response to potential therapeutics is challenging due to NO's short half-life and microglial heterogeneity. In this paper we report the application of a microfluidic device for the high-throughput measurement of intracellular NO in SIM-A9 microglial cells. NO production was measured in response to treatment with lipopolysaccharides (LPS) and interferon gamma (IFN-γ) with and without a potent iNOS inhibitor (1400W dihydrochloride). Cells were labeled with a fluorogenic NO probe, 4-amino-5-methylamino-2',7'-difluorofluoescein diacetate (DAF-FM DA), and 6-carboxyfluorescein diacetate (6-CFDA) as an internal standard. Separation and quantitation of intracellular NO was achieved using microchip electrophoresis and laser induced fluorescence detection (LIF). Statistical analysis suggests that the populations fit a lognormal distribution and are better represented by their geometric mean values. Comparison of the geometric means indicated a 1.6-fold increase in NO production between untreated and stimulated cells and a decrease by a factor of approximately 0.5 comparing stimulated and inhibited cells. Additionally, we report experimental data demonstrating the improvement in the sensitivity of our integrated optical fiber-based detection system through the use of refractive index matching gel.

Introduction

Current treatment strategies are largely ineffective for neurodegenerative diseases like Alzheimer's disease (AD), Parkinson's disease (PD), and chronic traumatic encephalopathy (CTE).[2-4] These diseases are characterized by accumulations of misfolded proteins in the brain which trigger a prolonged inflammatory response ultimately leading to neuronal death and a decline in cognitive or motor functions.[5] Microglia, being the resident immune cells in the brain, are responsible for the sustained inflammatory environment. Several reviews have cited studies that implicate microglia as playing a central role in the progression of these diseases and other brain pathologies.[5-9]

Microglial phenotypes can be described as resting/surveilling (M0), "classically" activated/pro-inflammatory (M1), or "alternatively" activated/anti-inflammatory (M2).[10] Under normal conditions, the microglial response to neurological insults in the central nervous system consists of a balance between the M1 and M2 phenotypes. A growing body of evidence suggests that microglia in aged brains become "hypersensitive" leading to exaggerated inflammation in response to the protein aggregates present in AD, PD, CTE and other pathologies.[11] Researchers have found that under these chronic inflammatory conditions, M1 activated microglia become neurotoxic causing accelerated neuronal death.[12] Upon M1 activation, microglia undergo changes in morphology and motility as they secrete pro-inflammatory cytokines like tumour necrosis factor alpha (TNF-α) and interleukin one beta (IL-1β), and other signalling molecules.[8, 12] One class of inflammatory signalling molecules produced by activated microglia are reactive nitrogen and oxygen species (RNOS). Among the RNOS produced, nitric oxide (NO) has received a lot of attention not only due to its involvement in several physiological processes but also because of its potentially harmful reactivity.[13] NO exists as a dissolved gas *in vivo* produced by a family of enzymes called nitric oxide synthases (NOSs). Inducible NOS (iNOS) is the isoform of NOS that is associated with the inflammatory phenotype of microglia. Excessive levels of NO can lead to nitrosative stress which can result in the induction of neuronal apoptosis thus accelerating the progression of neurodegeneration.[14] For this reason iNOS has become a potential therapeutic target for the treatment of neurodegenerative diseases.[15] Measuring NO production in

[a] *Department of Chemistry, Kansas State University, 1212 Mid-Campus Drive, 213 CBC Building, Manhattan, KS, USA. E-mail: culbert@ksu.edu*

microglial cells can help in evaluating the efficacy of novel therapies and may also serve as a means of studying the dynamics of microglial inflammation. However, it is difficult to obtain an accurate picture of NO levels in microglial cell populations not only due to its short half-life but also because most methods measure extracellular NO levels and are unable to account for cell-to-cell variations.[16, 17] Recently, advances in nanoelectrode techniques for the electrochemical detection of intracellular NO, and other RNOS, have been applied to the measurement of single cells.[18] However, these techniques are limited in throughput and are most useful in studying individual cells rather than larger cell populations.

Previously, our group has developed a microfluidic single cell analysis (SCA) device for the measurement of NO production in an immortalized T lymphocyte cell line (Jurkat).[19] NO levels were measured using a diaminofluorescein based probe (4-amino-5methylamino-2',7'-difluorofluorescein diacetate) or DAF-FM DA. More recently, we have improved the device by incorporating on-board pumping for cell transport and integrating an optical fibre that allows simultaneous detection at 2 locations in the device without additional optics or detectors.[20-22] Thus far, the SCA device has only been used for the analysis of Jurkat cells which are cultured in suspension, whereas the majority of vertebrate-derived cells are adherent. Furthermore, Jurkat cells are not an appropriate model cell line for the study of neurodegenerative diseases. Therefore, it was important that we demonstrate the application of this device to the measurement of a pathologically relevant biomolecule within a cell-type derived from the organ of interest. In this paper, we report the application of our SCA device for the analysis of NO in single microglial cells. As an in vitro cell line model, we chose the recently discovered spontaneously immortalized line of mouse microglial cells, SIM-A9.[23] The researchers that discovered this cell line compared them to primary microglia in terms of inflammatory response and phagocytic capacity. They concluded that SIM-A9 behave similarly enough to serve as a low-cost and readily available alternative to primary cells for in vitro studies of microglia. NO was measured under native conditions, and co-stimulation with lipopolysaccharides (LPS) and interferon gamma (IFN-γ) with and without a potent iNOS inhibitor (1400W dihydrochloride). Statistical analysis was performed on the fluorescence data for each cell population to characterize the shape of the population distribution, which highlights the usefulness of acquiring measurements with single-cell resolution. Additionally, we report improved optical fibre signal transmission through the use of refractive index matching gel (RI gel) to increase the sensitivity of our detection scheme.

Experimental

Materials and reagents

SIM-A9 microglial cells (mouse, ATCC CRL-3265) and Dulbecco's phosphate buffered saline (D-PBS, 1x ATCC 30-220) were purchased from American Type Culture Collection (Manassas, VA, USA). Dulbecco's Modified Eagle Medium/Nutrient Mixture F-12 (DMEM:F-12) was purchased from Thermo Fisher Scientific (Waltham, MA, USA). 4-Amino-5-methylamino-2',7'-difluorofluorescein diacetate (DAF-FM DA) was also purchased from Thermo Fisher Scientific in 50 µg packs. Sodium borate, lyophilized bovine serum albumin (BSA), Tween-20, xylenes (Certified ACS), acetonitrile (HPLC grade), and premium foetal bovine serum (USA origin, heat inactivated) were all obtained from Fisher Scientific (Pittsburgh, PA, USA). Sodium dodecyl sulphate, anhydrous dimethyl sulfoxide, 99.9% (DMSO), horse serum (USA origin, heat inactivated), and lipopolysaccharides (LPS) from *Escherichia* coli line 0111:B4 were purchased from Sigma-Aldrich (St. Louis, MO, USA). Lyophilized interferon gamma (IFN-γ) (Mouse) was purchased from GenScript (Piscataway, NJ, USA). 6-Carboxyfluorescein diacetate, single isomer (6-CFDA) and probenecid sodium salt were purchased from Biotium Inc. (Fremont, CA, USA). The iNOS inhibitor, 1400W dihydrochloride, was purchased from Tocris (Minneapolis, MN, USA). Negative tone photoresist SU-8 2010 was purchased from MicroChem Corp. (Newton, MA, USA). The SU-8 developer, 2-(1-methoxy) propyl acetate (99%), was obtained from Acros (Morris Plains, NJ, USA). AZ P4620 positive tone photoresist and AZ 400K developer (1:4) were obtained from AZ Electronic Materials (Branchburg, NJ, USA). Silicon wafers (100 mm diameter, single-side polished, mechanical grade or better) were purchased from Silicon, Inc. (Boise, ID, USA). Chrome coated (500 Å) silicon wafers (100 mm diameter, single-side polished, test grade) were purchased from WRS Materials (San Jose, CA, USA). (1,1,1,3,3,3-Hexamethyldisilazane (98%) (HMDS) was purchased from Gelest (Morrisville, PA, USA). Sylgard 184 PDMS prepolymer and curing agent were purchased from Dow Corning (Corning, NY, USA). Ultrapure water was generated from a Barnstead E-pure system (Dubuque, IA, USA). Multimode optical fibre (0.22 NA, core Ø105 µm) and refractive index matching gel (G608N3) were obtained from Thorlabs Inc. (Newton, NJ, USA).

Device fabrication

The SCA device was fabricated using photolithographically patterned silicon wafer masters (SWMs) and multilayer PDMS-based soft lithography as described in detail previously.[24] Briefly, the SCA device consists of 2 layers: the pumping layer (top) and the fluidic layer (bottom). Photomasks for each layer were made by submitting designs generated in AutoCAD 2019 (Autodesk, Inc., San Rafael, CA, USA) to a laser photoplotting company (Fineline Imaging, Colorado Springs, CO, USA) to be printed onto transparencies at a resolution of 40k dpi. The SWM for the pumping layer was patterned on a bare silicon wafer using the negative tone photoresist SU-8 2010 with a channel height of 20 µm. The fluidic layer SWM was patterned on a chrome coated silicon wafer using the positive tone photoresist AZ P4620 with a channel height of 18-20 µm.

Once the SWMs were made, the PDMS device was fabricated using multilayer soft lithography described in detail previously.[24] First, the fluidic layer was made by spin coating a 50 µm thick layer of PDMS onto the fluidic SWM. The pumping layer was made by pouring PDMS into a 5 mm thick plexiglass frame aligned on top of the fluidic SWM. Both layers were

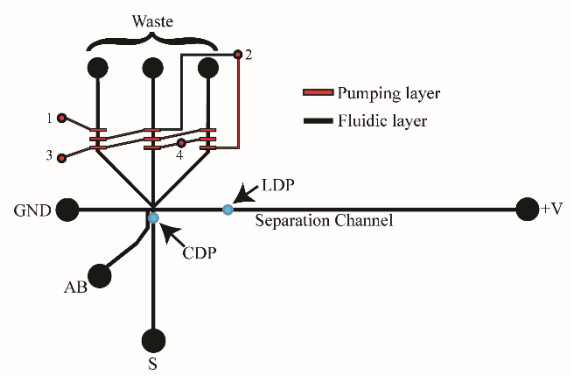

Fig. 1 A diagram of the fluidic and pneumatic microchannel manifolds. Positive and ground electrodes are placed into reservoirs labelled +V and GND respectively. The waste, auxiliary buffer (AB), GND and +V reservoirs are filled with electrophoresis buffer. Prepared cells are loaded into the sample buffer (S). The optical fibre ends are placed at the cell detection point (CDP) and the lysate detection point (LDP). Compressed air nozzles are placed into inlets in the pumping layer, labelled 1-4.

placed into an oven at 80 °C to cure for 90 min. Once cured, the layers were removed and allowed to cool. The pumping layer was then peeled off the pumping SWM and holes for compressed air inlets and the optical fibre were punched using a custom plexiglass jig as a guide. The pumping layer was placed on top of the fluidic layer by aligning the optical fibre holes with the fluidic channels for the cell detection point (CDP) and the lysate detection point (LDP) as shown in Fig. 1. The assembled layers were placed back into the 80 °C oven for an additional 90 min Once fully cured and cooled, the chip was then peeled off the fluidic SWM, and 3 mm diameter reservoir holes were punched out using a disposable biopsy punch.

Setup of device and LIF detection

For all experiments, an electrophoresis buffer, developed previously,[22] consisting of 0.2% Tween 20, 20% (v/v) acetonitrile, 20 mg/mL BSA, 2 mM SDS and 25 mM sodium borate was used. The device was prepared by gently rinsing the fluidic channels with ultrapure water and carefully drying with a compressed air blow gun. A 50x75 mm glass microscope slide was cleaned using a cleanroom swab and glassware soap followed by thorough rinsing with ultrapure water and subsequent drying using compressed air. The device was then reversibly sealed to the glass slide being careful to avoid trapping air bubbles. All channels were then filled with electrophoresis buffer. Platinum wire electrodes were placed into the "GND" and "+V" reservoirs, and compressed air nozzles were inserted into the inlets for the on-chip pumping manifold.

The on-board pumps function by actuating the valves in a pattern that results in peristalsis causing a net movement of fluid toward the waste reservoirs. This was achieved by connecting a regulated compressed air source to 4 solenoid valves mounted on a manifold (The Lee Company, Westbrook, CT, USA). The valve actuation pattern was controlled using a programmed microcontroller (pro trinket 5V, Adafruit, New York City, NY, USA). The flow rate driven by the pumps can be adjusted by increasing or decreasing the actuation pressure using a regulator. The relationship between actuation pressure and resulting flow rate was characterized previously.[22]

The LIF detection setup consisted of a 488 nm laser (Oxxius-LBX-488-100-CSB-PP) directed through the rear port of an inverted microscope (Nikon TS-100-F, Nikon Instruments Inc., Melville, NY, USA). The beam was directed upward into a 20x microscope objective (NA = 0.45) via a fluorescence filter cube (XF115-2 FITC, Omega Optical, Battleboro, VT, USA). Fluorescence emission was detected by a PMT (R-928, Hamamatsu Instruments, Bridgewater, NJ, USA). The signal current from the PMT was amplified (50 µA/V) and filtered (30 Hz, low-pass) using a low-noise current preamplifier (Stanford Research Systems, Sunnyvale, CA). The analogue voltage output was recorded using the 16-bit analogue input of a USB analogue to digital converter (USB-6002, National Instruments, Austin, TX, USA) connected to a computer running an in-house written LabVIEW program (National Instruments).

Preparation and set up of the optical fibre detection is detailed elsewhere.[20, 21, 24] Briefly, the optical fibre is coupled to the chip using two 23-gauge needles with both ends cut off. A small amount of refractive index matching gel (RI gel) was applied to one end on each of the needles, and then they were inserted into the punched optical fibre holes in the device. A length of optical fibre (approx. 20 cm) was cut and each end was cleaved to ensure that the fibre faces were smooth (FC-6S, Sumitomo Electric Lightwave Corp., Raleigh, NC, USA). Both ends were cleaned using an isopropanol soaked optical wipe and then carefully inserted into the needles until the fibre face touched the membrane above the fluidic channels below (shown in Fig. 2A). The optical fibre detection spots were aligned and secured using custom 3D printed aligning tools shown in Fig. 2B.

Tissue culture

SIM-A9 cells were cultured lying flat in T75 polystyrene flasks (Fisher Scientific, Waltham, MA, USA) in a humidified environment at 37 °C and 5% CO_2 in Dulbecco's Modified Eagle Medium/Nutrient Mixture F-12 (DMEM:F-12) supplemented with heat inactivated foetal bovine serum (10% v/v), heat inactivated horse serum (5% v/v), and streptomycin (100 µg/mL). Once the cells reached 80% confluency, they were passaged. SIM-A9 cultures contain a mixture of adhered and suspended cells. Passaging begins by first scraping the attached cells using an in-house made glass scraper. Scraped cells and suspended cells were then mixed by pipetting and transferred to a 15 mL conical vial and centrifuged at 1000 rpm (or 125 x g) for 5 min. The supernatant was then discarded, and the cell pellet was resuspended in fresh media and split into flasks at a subcultivation ratio between 1:3 and 1:6 with a total culture volume of 15 mL.

Stimulation and inhibition of NO production

Stimulation of NO production was induced by cotreating cells with purified lipopolysaccharides (LPS) and recombinant mouse interferon gamma (IFN-γ). Stock solutions of LPS and IFN-γ were prepared in PBS at concentrations of 1 mg/mL and 100 µg/mL respectively. Aliquots of both solutions were stored frozen at -20 °C until ready for use. All experiments were performed using cell cultures that had reached 80% confluency. For stimulation experiments, LPS and IFN-γ were added to the

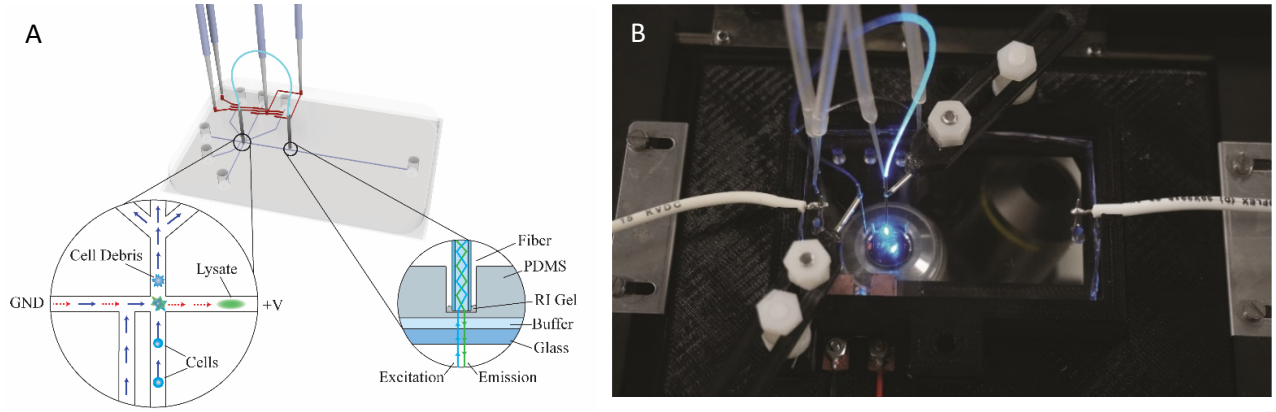

Fig. 2 (A) A 3D rendering of the SCA device with the integrated optical fiber with diagrams illustrating the lysis mechanism (left) and the optical path that the excitation and emission light travels (right). The red dotted arrows in the lysis diagram represent electrophoretic flow and the blue solid arrow represent the hydrodynamic flow driven by on-board pumps. (B) A photograph of the assembled SCA system in the custom 3D printed stage plate.

cell culture flask yielding final concentrations of 500 ng/mL and 50 ng/mL respectively. The flask was then placed back into the incubator at 37 °C and 5% CO_2 and incubated for 4 hr prior to NO measurement. For inhibition experiments, cells were treated with the same amounts of LPS and IFN-γ with the addition of a selective iNOS inhibitor, 1400W dihydrochloride, at a concentration of 100 µM. The cells were then incubated for the same time and under the same conditions as the stimulation experiments. Cells used for measuring native NO levels were left untreated.

Sample preparation

Intracellular NO levels were measured by co-labelling cells with DAF-FM DA and internal standard 6-CFDA following a similar procedure described previously.[24] Stock solutions of DAF-FM DA (approx. 1 mM) and 6-CFDA (3.74 mM) were prepared in anhydrous DMSO and were aliquoted and stored frozen at -20 °C until ready for use. Additionally, to minimize dye efflux by MRP1 a 250 mM stock solution of probenecid, an MRP1 inhibitor,[25] was prepared in PBS. A labelling solution containing 6-CFDA (40µM), DAF-FM DA (150 µM) and probenecid (2.5 mM) was prepared fresh for each experiment in PBS. The experimental procedure for treatment and preparation of cells is illustrated in Fig. 3. Once the cells were ready for NO measurements, native, stimulated, and inhibited cells were all treated in the following manner. Cells were first scraped and mixed as described above. A sample of the cell suspension (1 mL) was then transferred into a 1.5 mL Eppendorf tube and centrifuged (1000 rpm for 5 min). The supernatant was then removed, and the pellet was resuspended in 100 µL of the labelling solution and incubated for 30 min at 37 °C on a dry bath heating block. Following labelling, the cells were diluted to 1 mL with prewarmed PBS (37 °C) and centrifuged (1000 rpm, 5 min). The supernatant was then discarded, and the cells were resuspended again in 1 mL of prewarmed PBS. The cells were spun down and resuspended twice more, but the final resuspension solution was 1 mL of PBS containing 2 mg/mL BSA and 2.5 mM probenecid.

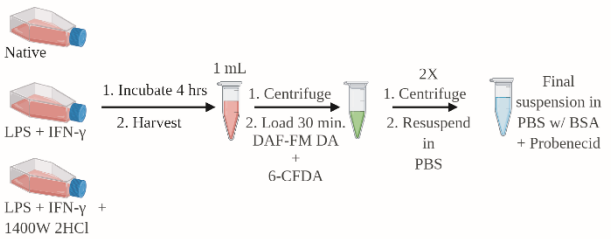

Fig. 3 A scheme illustrating the procedure used to prepare cells for NO measurements. Created using Biorender.com.

Microchip operation

The buffer in the sample reservoir (labelled "S" in Fig. 1) is replaced with 30 µL of cell suspension. Cells are then drawn toward the lysis intersection by the on-board pumps. As the cells pass underneath the CDP, excitation light from the fibre excites the intracellular probes, and the fluorescence is transmitted back through the fibre and into the optical detection system. The cells then enter the lysis intersection where they experience a high electric field (850 V/cm) which permanently disrupts the cellular membrane, and the cytosolic contents are injected into the separation channel. The injected contents are then electrophoretically separated and the fluorescence emission peaks for each of the probes is detected downstream at the LDP. A diagram illustrating the cell transport and lysis is shown in Fig. 2A, and a typical electropherogram with each fluorescent peak labelled is shown in Fig. 4A.

Results and discussion

Over the years, our research group has published several reports on the continued development of this high-throughput microfluidic single cell analysis technology.[19-22, 24] However, this is the first demonstration of our system being used for the analysis of an adherent cell type and examining the effects of the addition of stimulators in combination with inhibitors to measure cell response.

Signal enhancement

One limitation to the optical fibre bridge that was discussed in its initial reporting was the loss of signal due to fibre coupling inefficiency.[20] It is likely that signal loss can be attributed to Fresnel reflection at the fibre-membrane interface due to the presence of small air gaps between the optical fibre face and the PDMS membrane. Additionally, scattering may also contribute to lost signal because of imperfections (such as

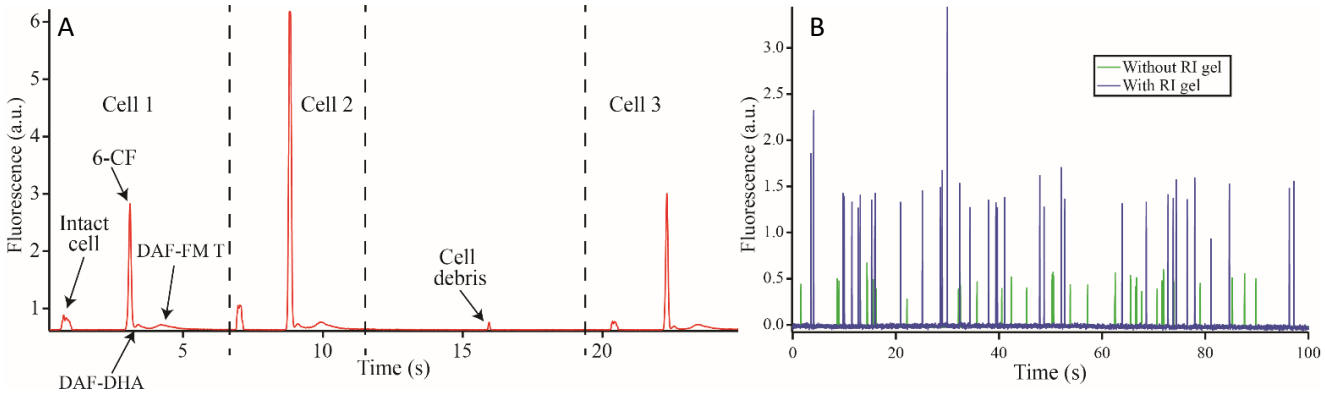

Fig. 4 (A) A representative excerpt of fluorescence data for single cell analysis of NO. Each cell produced a total of 4 peaks: intact cell, 6-CF, DAF-DHA and DAF-FM T. (B) Fluorescence signal from 10 µm fluorescent polystyrene microspheres with RI gel (blue) and without (green).

scratches) in the fragile PDMS membrane. In the telecommunications industry, a refractive index matching liquid or gel is commonly used for fibre couplings to mitigate similar issues that occur at fibre junctions.

For our experiments, we applied small amounts of a RI gel to both ends of the optical fibre bridge before inserting them into the microfluidic device. To compare the transmission efficiency of the optical fibre with and without the RI gel, we loaded a sample of fluorescent 10 µm diameter polystyrene microspheres into the sample reservoir and pulled them past the CDP using the on-board pumps and measured the emission at the LDP. Plots showing a series fluorescence peaks both with and without RI gel is shown in Fig. 4B. The average fluorescence signals for both conditions are shown in Table 1. With the RI gel, we observed a 200% improvement in signal.

Measurement of NO production

SIM-A9 cells are a recently isolated spontaneously immortalized cell line, and as such, there are relatively few studies available for comparing results. However, initial comparisons between SIM-A9 cells and their primary counterparts indicate that they behave similarly in response to inflammatory stimuli.[23]

For stimulation experiments, cells were co-stimulated with LPS and IFN-γ for 4 hr to elicit an inflammatory response which is characterized, in part, by elevated levels of NO production. For inhibition experiments, cells were incubated with the same levels of LPS and IFN-γ for the same period of time but in the presence of the potent and selective iNOS inhibitor 1400W dihydrochloride. Cells for native, stimulated, and inhibited experiments were then all treated in the same manner prior to analysis, shown as a workflow in Fig. 3. Cells were incubated in a loading solution containing the fluorogenic NO probe, DAF-FM DA, and an internal standard, 6-CFDA. 6-CFDA has been used as an internal standard for similar analyses previously.[19, 26] Once inside the cell, both DAF-FM DA and 6-CFDA are hydrolysed by non-specific esterases to form DAF-FM and 6-CF, respectively. This allows us to account for cell-to-cell variability in cell volume, esterase activity and viability.

Table 1 Average intensity and 95% confidence interval of fluorescence signals from 10 µm fluorescent microspheres with and without the application of RI gel to the optical fibre faces.

	n	Average Intensity (a.u.)
Without gel	80	0.48±0.03
With gel	80	1.43±0.09

The optical fibre detection was set up such that the CDP was just below the lysis intersection and LDP was 2 mm down the separation channel. The on-board pumps were then turned on to draw the cells to the lysis intersection. An electric field strength of 850 V/cm was applied across the separation channel providing a means of lysis and subsequent electrophoretic separation of the intracellular contents. The flow rate, driven by the pumps, was adjusted at the beginning of each experiment to achieve optimal cell lysis and injection efficiency. The conditions for maximum injection efficiency were determined by visually observing lysis and adjusting the flow rate up or down such that ~100% of the lysate travels down the separation channel and the cell debris travels toward the waste reservoirs.

As cells flow underneath the CDP, a short and narrow peak is observed followed shortly by a set of peaks corresponding to 6-CFDA, DAF-DHA and DAF-FM T as they pass the LDP. A representative excerpt showing a series of single cell electropherograms is shown in Fig. 4A. Intracellular NO production was calculated for each cell using the ratio of the peak area of DAF-FM T (A_{DAF}) to the peak area of the internal standard 6-CF (A_{CF}). The population distributions of NO production for each experiment were visualized using histograms shown in Fig. 5. The shape of each distribution was characterized by computing the skewness and subsequently testing for normality using a Shapiro-Wilk test.[27] The skewness values for all three distributions were significantly positive indicating that the majority of cells fall in the lower end of the distribution with the presence of a tail toward higher values (shown in Table 2). The Shapiro-Wilk test P-values confirmed that the distributions could not be described as normal (α = 0.05). These results initially precluded the use of a one-tailed t-test for the comparison of means of independent samples because the assumption of normality was not met. However, given the positive skewness and the absence of negative values, we theorized that the data may fit a lognormal distribution. To test the data for lognormality, a log transformation was

Table 2 Skewness and Shapiro-Wilk P-values for untransformed and log transformed datasets for native, stimulated, and inhibited conditions

	Untransformed		Transformed	
	Skewness [a]	Shapiro-Wilk P-value [b]	Skewness [a]	Shapiro-Wilk P-value [b]
Native	4.43	$4.5\text{x}10^{-14}$	0.083	0.25
Stimulated	2.99	$1.72\text{x}10^{-09}$	0.41	0.28
Inhibited	1.63	$1.12\text{x}10^{-08}$	-0.31	0.39

[a] Skewness is calculated as: $\frac{n}{(n-1)(n-2)}\sum\left(\frac{x_i-\bar{x}}{s}\right)^3$

[b] A high Shapiro-Wilk P-value indicates a good fit for a normal distribution. If $P \geq \alpha = 0.05$ for the log transformed data, then the null hypothesis that the distribution is lognormal fails to be rejected.

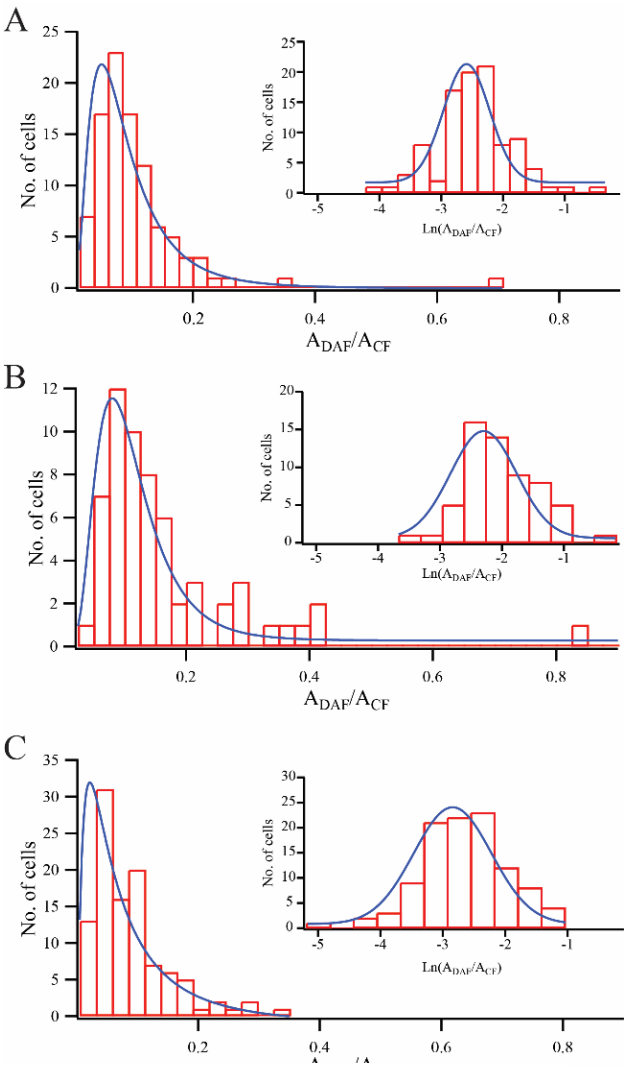

Fig. 5 Histogram plots of the peak area ratios for native (A), stimulated (B), and inhibited (C) conditions. The insets in A-C are histogram plots for the log transformed datasets. The traces are lognormal fits for the main plots and gaussian for the inset plots.

performed on each dataset (using the natural logarithm), and the skewness and Shapiro-Wilk test were repeated. The skewness of the log transformed data was significantly reduced, and the Shapiro-Wilk test confirmed that the log transformed data were normally distributed ($\alpha = 0.05$). The mean values of the log transformed datasets could then be compared using a one-tailed t-test for the comparison of means of independent samples. First, the standard deviations for the transformed native, stimulated and inhibited datasets were compared using an F test to determine which form of the t-test was appropriate. The calculated F statistics (F_{calc}) for each comparison concluded that the standard deviations were not significantly different ($\alpha = 0.05$). The means of the transformed data sets were then compared, and the calculated t values indicated that the differences were statistically significant. The p-values for each comparison are listed in Table 3. While confidence intervals for normal distributions are symmetrical about the arithmetic mean, lognormal distributions are better represented using the geometric mean with an asymmetrical confidence interval based on the multiplicative standard deviation. The geometric mean ($\bar{x}^*$) and multiplicative standard deviation (s^*) are determined by "back-transforming" the mean ($\bar{x}$) and standard deviation (s) of the transformed data[1]:

$$\bar{x}^* := e^{\bar{x}}, \quad s^* := e^{s}$$

Table 3 Arithmetic and geometric summary statistics for native, stimulated, and inhibited datasets.

	n	$\bar{x} \pm s$	$\bar{x}^* \,{}^{x}\!/\, s^*$	~95% C.I.*
Native	97	0.10±0.08	0.085 ˣ/1.83	0.025-0.28
Stimulated	60	0.16±0.13	0.133 ˣ/1.86	0.038-0.46
Inhibited	105	0.088±0.063	0.070 ˣ/2.02	0.017-0.28

*The $^{x}\!/$ for geometric statistics is analogous to the ± for arithmetic statistics. The lower and upper bounds of the 95% confidence interval are: $\bar{x}^* \div s^{*2}$ and $\bar{x}^* \times s^{*2}$.[1]

Table 4 Calculated % differences in the peak area ratios between each experimental condition. The p-values listed correspond to the one-tailed t-test for the comparison of means of independent samples performed on the log

	%diff. (p-value)
Native-Stimulated	+56% (p<0.00001)
Stimulated-Inhibited	-47% ($p<2x10^{-8}$)
Native-Inhibited	-18% (p<0.02)

Table 3 shows the summary statistics for the native, stimulated and inhibited experiments and includes both the arithmetic mean and standard deviation as well as the geometric mean and multiplicative standard deviation. An overlay of representative single cell electropherograms for the native, stimulated, and inhibited experiments is shown in Fig. 6. The fluorescent peak heights were adjusted according to the internal standard, 6-CF, to allow for a direct comparison of cells. To compare the change in NO production across the cell populations, the percent difference between each experimental condition was calculated using the geometric mean values (shown in Table 4). It is worth noting that despite the fact that the NO levels are not being measured in units of concentration, this method still produces a numerical measure that will enable researchers to quantitatively study the impact of various pharmacological agents on cellular populations.

When comparing the various conditions, we observed a 56%($p<0.00001$) increase in NO production between the native and stimulated experiments and a 47%($p<2x10^{-8}$) decrease in NO production when cells were simultaneously treated with iNOS agonists (LPS and IFN-γ) and the iNOS inhibitor (1400W dihydrochloride). We also observed a modest decrease in NO production (approx. 18%, $p<0.02$) in the inhibited cell population as compared to the native cell population. It is likely that during the course of the cell harvesting and loading processes an acute inflammatory response was elicited as a result of incidental cellular stress and damage. In future studies more gentle handling and loading techniques will be investigated to minimize their impact on measurements of inflammatory markers. It is also possible that the iNOS enzyme could produce more NO to compensate for the NO that was consumed by the reaction with DAF-FM. This would result in a gradual increase in DAF-FM T signal over the course of an experiment. Fortunately, we did not observe this phenomenon under any of the experimental conditions.

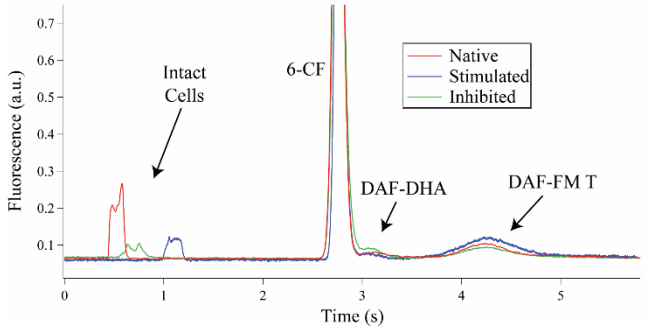

Fig. 6 An overlay of single cell electropherograms for native, stimulated, and inhibited cells. The fluorescence intensities have been scaled according to the internal standard peak signal.

One potential downside to measuring NO using diaminofluorescein species, discussed in our previous publication,[19] is the formation of fluorescent derivatives when reacted with dehydroascorbate (DHA), the oxidized form of ascorbic acid (AA). AA interference is of particular concern when measuring NO production in microglia because AA concentrations in the brain parenchyma (2-10 mM) are among the highest in the body.[28] Comparing our electropherograms to those reported previously, we believe that the second peak is a DAF-DHA derivative (Fig. 4 and 8).[26] Some studies have suggested that AA levels may play a role in chronic neuroinflammation associated with neurodegenerative pathologies.[29, 30] In future experiments, we may exploit the formation of DAF-DHA derivatives as a means to measure intracellular AA levels and its impact on inflammation.

Single vs bulk cell analysis

Without the benefit of a large number of studies, it is difficult to compare our results to any published reports. Additionally, all NO analyses reported for SIM-A9 microglia thus far were bulk cell measurements of extracellular NO levels using the Griess reaction.[23] Using DAF-FM DA instead of the Griess reaction not only provides greater sensitivity, but allows for the quantitation of intracellular NO production at the single cell level which can yield more detailed information about how a population of cells respond to pro-inflammatory stimuli. In bulk-cell studies, the population average values measured are not capable of determining the shape of the distribution of cellular response. Recent studies show that measuring cellular response at the single-cell level can help to better characterize the regulatory roles that signalling enzymes and molecules play.[31, 32] Mapping the different regulatory roles of signalling components in a cascade may help to better understand how normal cellular function is disrupted, especially in neurodegenerative pathologies. With this information, novel treatment strategies may be developed to combat the disruptions more specifically. Furthermore, the efficacy of the new treatment strategies can be evaluated using the same single-cell analysis technologies used to study the signalling cascades.[33]

Conclusion

In our recent publication, we integrated an optical fibre into the device allowing for fluorescence detection at two locations on the device with no additional optics.[20] Here we demonstrated an improvement in the optical fibre detection through the use of RI gel to minimize signal loss due to scattering and retroreflection. Fluorescent beads were used to measure the impact of the RI gel on signal intensity and a 3-fold increase in signal on average was observed. We hope that this improvement in sensitivity will allow the quantitation of analytes at lower concentrations while maintaining the ability to detect an intact cell signal. We then used the microfluidic device to measure changes in NO levels in SIM-A9 microglial

cells under native, stimulated, and inhibited conditions using a fluorogenic probe and an internal standard. Following a 4-hr stimulation with LPS and IFN-γ, a 56% increase in NO production was observed as compared to native cells. The effects of a selective iNOS inhibitor, 1400W dihydrochloride, were measured by treating cells with both the inflammatory stimulants and the inhibitor. Not only were NO levels lower than stimulated conditions by approximately 47%, but inhibited cells produced 18% less NO compared to native cells. In addition to quantitation, the electrophoretic separation allowed us to distinguish between fluorescence from DAF-FM T and the interfering DHA derivatives. We also observed that the population distributions for all three experimental conditions exhibited lognormal characteristics. Further characterization of cell-to-cell variability in the expression and production of inflammatory markers may help to better understand the impact aging has on the immune system. It is worth noting that this is the first report of single cell analysis being performed on SIM-A9 microglial cells. This report marks the first instance of our device's application for the analysis of an adherent cell line since the beginning of its development in 2003.[34] We hope to further expand the application of our device to the analysis of other cell types relevant to other brain diseases, such as U-87 glioblastoma cells. Future work will be directed toward studying how glioblastoma cells modulate nearby immune cells to promote tumour growth and survival. We will also work toward incorporating additional fluorescent reporters for other reactive oxygen and nitrogen species including peroxynitrite and superoxide to gain a more comprehensive picture of the effects of chronic neuroinflammation.

Conflicts of interest

There are no conflicts of interest to declare.

Acknowledgements

This research was funded by NSF Grants CBET-1933321, CBET-1894416, and CBET-1656968.

Notes and references

1. E. Limpert, W. A. Stahel and M. Abbt, *BioScience*, 2001, **51**, 341-352.
2. J. Weller and A. Budson, *F1000Res*, 2018, **7**.
3. P. Maiti, J. Manna and G. L. Dunbar, *Transl Neurodegener*, 2017, **6**, 28.
4. H. M. Makinde, T. B. Just, C. M. Cuda, H. Perlman and S. J. Schwulst, *Shock*, 2017, **48**, 276-283.
5. M. V. Guillot-Sestier and T. Town, *J Neural Transm (Vienna)*, 2018, **125**, 751-770.
6. C. Arcuri, B. Fioretti, R. Bianchi, C. Mecca, C. Tubaro, T. Beccari, F. Franciolini, I. Giambanco and R. Donato, *Front Biosci (Landmark Ed)*, 2017, **22**, 268-309.
7. A. C. da Fonseca, R. Amaral, C. Garcia, L. H. Geraldo, D. Matias and F. R. Lima, *Adv Exp Med Biol*, 2016, **949**, 245-261.
8. J. A. McKenzie, L. J. Spielman, C. B. Pointer, J. R. Lowry, E. Bajwa, C. W. Lee and A. Klegeris, *Curr Aging Sci*, 2017, **10**, 158-176.
9. G. A. Elder, M. E. Ehrlich and S. Gandy, *Neurosci Lett*, 2019, **707**, 134294.
10. C. Sousa, K. Biber and A. Michelucci, *Front Immunol*, 2017, **8**, 198.
11. K. Biber, T. Owens and E. Boddeke, *Glia*, 2014, **62**, 841-854.
12. F. L. Heppner, R. M. Ransohoff and B. Becher, *Nat Rev Neurosci*, 2015, **16**, 358-372.
13. F. X. Guix, I. Uribesalgo, M. Coma and F. J. Munoz, *Prog Neurobiol*, 2005, **76**, 126-152.
14. G. C. Brown and A. Bal-Price, *Mol Neurobiol*, 2003, **27**, 325-355.
15. J. E. Yuste, E. Tarragon, C. M. Campuzano and F. Ros-Bernal, *Front Cell Neurosci*, 2015, **9**, 322.
16. J. M. Siegel, K. M. Schilly, M. B. Wijesinghe, G. Caruso, C. G. Fresta and S. M. Lunte, *Anal Methods*, 2019, **11**, 148-156.
17. W. S. Kim, X. Ye, S. S. Rubakhin and J. V. Sweedler, *Anal Chem*, 2006, **78**, 1859-1865.
18. K. Hu, Y.-L. Liu, A. Oleinick, M. V. Mirkin, W.-H. Huang and C. Amatore, *Current Opinion in Electrochemistry*, 2020, **22**, 44-50.
19. E. C. Metto, K. Evans, P. Barney, A. H. Culbertson, D. B. Gunasekara, G. Caruso, M. K. Hulvey, J. A. Fracassi da Silva, S. M. Lunte and C. T. Culbertson, *Anal Chem*, 2013, **85**, 10188-10195.
20. D. E. Patabadige, J. Sadeghi, M. Kalubowilage, S. H. Bossmann, A. H. Culbertson, H. Latifi and C. T. Culbertson, *Anal Chem*, 2016, **88**, 9920-9925.
21. J. Sadeghi, D. E. Patabadige, A. H. Culbertson, H. Latifi and C. T. Culbertson, *Lab Chip*, 2016, **17**, 145-155.
22. D. E. Patabadige, T. Mickleburgh, L. Ferris, G. Brummer, A. H. Culbertson and C. T. Culbertson, *Electrophoresis*, 2016, **37**, 1337-1344.
23. K. Nagamoto-Combs, J. Kulas and C. K. Combs, *J Neurosci Methods*, 2014, **233**, 187-198.
24. J. Sibbitts, J. Sadeghi and C. T. Culbertson, *Methods Enzymol*, 2019, **628**, 223-241.
25. F. Di Virgilio, T. H. Steinberg and S. C. Silverstein, *Cell Calcium*, 1990, **11**, 57-62.
26. E. R. Mainz, D. B. Gunasekara, G. Caruso, D. T. Jensen, M. K. Hulvey, J. A. Fracassi da Silva, E. C. Metto, A. H. Culbertson, C. T. Culbertson and S. M. Lunte, *Anal Methods-Uk*, 2012, **4**, 414-420.
27. S. S. Shapiro and M. B. Wilk, *Biometrika*, 1965, **52**, 591-611.
28. F. E. Harrison and J. M. May, *Free Radic Biol Med*, 2009, **46**, 719-730.
29. X. Y. Zhang, Z. P. Xu, W. Wang, J. B. Cao, Q. Fu, W. X. Zhao, Y. Li, X. L. Huo, L. M. Zhang, Y. F. Li and W. D. Mi, *Int Immunopharmacol*, 2018, **65**, 438-447.
30. C. C. Portugal, R. Socodato, T. Canedo, C. M. Silva, T. Martins, V. S. Coreixas, E. C. Loiola, B. Gess, D. Rohr, A. R. Santiago, P. Young, R. D. Minshall, R. Paes-de-Carvalho, A. F. Ambrosio and J. B. Relvas, *Sci Signal*, 2017, **10**.
31. O. Feinerman, J. Veiga, J. R. Dorfman, R. N. Germain and G. Altan-Bonnet, *Science*, 2008, **321**, 1081-1084.
32. Y. Lu, A. Biancotto, F. Cheung, E. Remmers, N. Shah, J. P. McCoy and J. S. Tsang, *Immunity*, 2016, **45**, 1162-1175.
33. M. Niepel, S. L. Spencer and P. K. Sorger, *Curr Opin Chem Biol*, 2009, **13**, 556-561.

34. M. A. McClain, C. T. Culbertson, S. C. Jacobson, N. L. Allbritton, C. E. Sims and J. M. Ramsey, *Anal Chem*, 2003, **75**, 5646-5655.

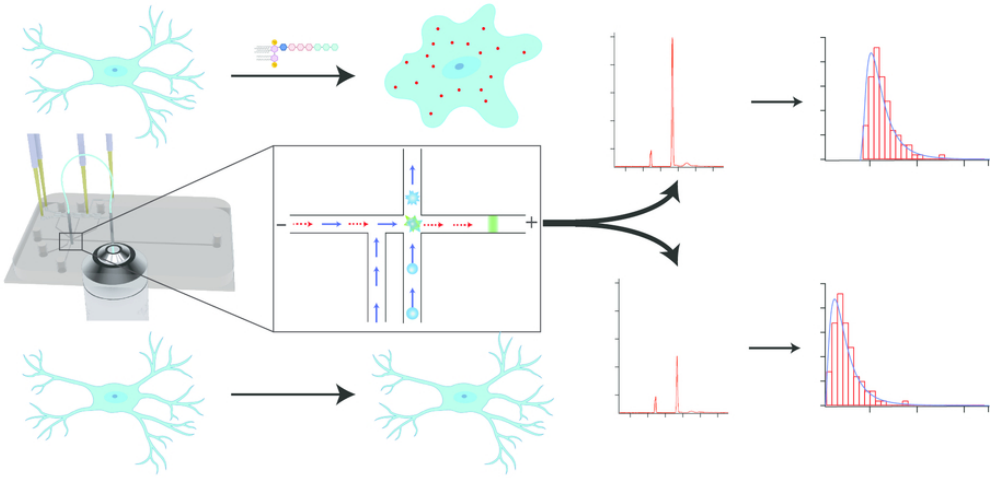

A microfluidic single cell analysis device was used to measure the distribution of nitric oxide levels in SIM-A9 microglial cell populations in response to stimulation and inhibition of inducible nitric oxide synthase.

77x38mm (300 x 300 DPI)